



Nano- and micro-indentation testing of sintered UO_2 fuel pellets with controlled microstructure and stoichiometry



Bowen Gong^a, David Frazer^d, Tiankai Yao^a, Peter Hosemann^b, Michael Tonks^c,
Jie Lian^{a,*}

^a Department of Mechanical, Aerospace, Nuclear Engineering, Rensselaer Polytechnic Institute, Troy, NY, 12180, USA

^b Nuclear Engineering Department, University of California, Berkeley, CA, 94720, USA

^c Department of Materials Science and Engineering, University of Florida, 158 Rhines Hall, Gainesville, FL, 32611, USA

^d Material Science and Technology Division, Los Alamos National Laboratory, Los Alamos, NM, USA

ARTICLE INFO

Article history:

Received 6 November 2018

Received in revised form

19 December 2018

Accepted 14 January 2019

Available online 16 January 2019

ABSTRACT

Dense nanocrystalline and microcrystalline UO_2 samples with controlled grain structure and stoichiometry were prepared by high energy ball milling and spark plasma sintering (SPS). Nano-indentation and micro-indentation testing were performed at different temperatures of 25 °C, 300 °C, and 600 °C in order to study the mechanical properties of the sintered fuels as functions of grain structure and temperature. Nanocrystalline UO_2 display higher hardness than microcrystalline counterpart, consistent with the Hall-Petch strengthening mechanism. Greater Young's modulus and fracture toughness are also identified for the nanocrystalline UO_2 , and hardness and Young's modulus decrease with temperature, suggesting better ductility of oxide fuels at high temperature and small length scale. Hyperstoichiometric UO_2 specimen displays higher hardness and fracture toughness than stoichiometric UO_2 , due to the impediment of the crack propagation by the oxygen interstitial atoms. These results are useful in understanding the mechanical properties of the high burn-up structure (HBS) formed in nuclear fuels during reactor operation, and also provide critical experimental data as the input for the development and validation of the MARMOT fracture model of nuclear fuels.

© 2019 Elsevier B.V. All rights reserved.

1. Introduction

Uranium dioxide (UO_2) has been widely used as a major nuclear fuel form in boiling water reactor (BWR) and pressurized water reactor (PWR) because of its stability [1] and outstanding corrosion resistance [2]. When the fuel pellet is burned in the reactor, a significant temperature gradient is generated across the fuel pellets. Meanwhile, fission products with kinetics energy of 100 MeV will generate thermal spikes [3] and collision cascade, contributing to the drastic microstructural defects and evolution. A high burn-up structure (HBS) starts to form at the outer region of the nuclear fuel pellets when the burnup reaches ~50 GWd/tHM and fully transforms at ~75 GWd/tHM [4,55,56]. In this region, microcrystalline (referred as mc-hereafter) grains subdivide from 10 to 15 μm into nanocrystalline (referred as nc-hereafter) grains with an

average grain size of several hundreds of nano-meters. Nc-materials usually exhibit superior mechanical properties than the conventional coarsen-grain materials, such as higher hardness [5,6], strength [6–8], improved thermal diffusivities [9] and electrical resistivity [10]. However, the mechanism behind the enhanced properties is still under debate. Hall derived the relationship of strength and hardness with grain size based on the pile up of the dislocations close to grain boundaries [11], which did not work well for structures with grain size smaller than a certain threshold [57], generally 10 to 20 nm [58,59]. A new mechanism of volume fraction of triple junctions [12] was later proposed to explain the hardness and strength drop when the grain size is beyond the threshold.

To mimic the HBS morphology and compare its properties with mc- UO_2 at different temperatures, high density nc- UO_2 and mc- UO_2 pellets with controlled microstructure and stoichiometry are desired. Traditionally, the synthesis of bulk UO_2 pellets involves high temperature sintering, e.g., above 1700 °C for hours. Amato et al. [13] reported over 95% theoretical density (TD) using hot-pressing at 4000–8000 psi and 1100–1400 °C, ranging from 10 to

* Corresponding author.

E-mail address: lianj@rpi.edu (J. Lian).

60 mins. Yang et al. adopted microwave sintering in H₂ atmosphere at 1600 °C for an hour [14]. The grain size of the pellets synthesized ranges from several to dozens of microns. Recently, rapid consolidation method has been widely used to sinter ceramic materials in a short period, effective to sinter bulk pellets with a nano-sized grain structure. Spark plasma sintering (SPS) is an example of rapid consolidation, which utilizes high DC current to enable the consolidation and the synthesis of the material. As a result of rapid consolidation of materials at short duration and lower temperature, the grain structure of the starting materials can be well preserved upon sintering without significant grain growth, enabling the densification of nanoceramics. Microstructure of the densified materials can also be controlled by adjusting the SPS sintering parameters such as temperature, pressure, and holding time during sintering. Ge et al. has studied the effects of the variation of these parameters on the densification, grain size, and hardness of UO₂ [2]. SPS has been adopted to many materials, such as nc-ZrO₂ (3Y) [14], nc-(UO₂, SiC) compound [14], nc-UO₂ [15] and mc-UO₂ [16].

Microindentation and nanoindentation are typically used to test mechanical properties of materials such as hardness [17–20], elastic modulus [21,22], and fracture toughness [17,23]. Micro-indentation testing method is commonly used to measure material hardness on a microscopic scale utilizing a precision diamond indenter to penetrate the materials surface and produce an impression. Microhardness can be calculated based on the load and the area of the impression. On the other hand, nanoindentation employs a more precise tip to press the material and produce an indentation area of several square micrometers or even less, and hence can be used on thin film and small volumes. During the testing, the load and displacement data are continuously recorded, allowing the calculation of Young's modulus and many other mechanical properties.

In this paper, we present a systematic study of materials sintering by SPS and mechanical testing of the sintered UO₂ with controlled microstructure and stoichiometry in which the nano-sized UO₂ can mimic the HBS with a comparable length scale of hundreds of nano-meters. Microindentation and nanoindentation were performed in order to understand the mechanical properties of the sintered UO₂ as functions of grain structures and temperatures. The main results derived from nanoindentation include hardness and Young's moduli for UO₂ with various grain sizes at room temperature (referred as RT hereafter), 300 °C, and 600 °C. The results obtained from microindentation include hardness and fracture toughness for the fuels with different stoichiometry and grain size at RT. The experimental data acquired are compared with values in the literature and will also be fed to the NEAMS tool to develop MARMOT fracture models.

2. Experimental procedure

2.1. Sintering UO₂ with controlled microstructure and stoichiometry

The dense UO₂ ceramics with different microstructure and grain size were fabricated by the combination of high energy ball milling (HEBM) and Spark Plasma Sintering (SPS) following the procedure reported in Ref. [24]. Specifically, polycrystalline UO₂ fuel pellets with different grain sizes (7.2 and 1.5 μm and 125 nm) were sintered by SPS from various batches of powder samples prepared from UO_{2.16} powders purchased from International Bio-analytical Industries Inc. USA. Ball milling of the as-received powders was conducted to decrease the particle size and enhance sinterability. Chemical reduction of the starting powders with UO_{2.16} was also performed to reduce the stoichiometry to UO_{2.03}.

Large-sized UO₂ pellets with a grain size of 7.2 μm were sintered directly from the as-purchased UO_{2.16} powder at 1600 °C for 5 mins

under a pressure of 40 MPa. The pellets with a grain size of 1.8 μm were sintered from nanocrystalline UO_{2.03} powders at 1300 °C for 30 mins under a pressure of 40 MPa. Due to the graphite die used in those two sintering routes, the pellets were *in-situ* reduced to hypo-stoichiometric. The pellets with a grain size of 125 nm were sintered at 700 °C for 5 mins under a pressure of 500 MPa in WC die. The densified nano-sized pellets are hyperstoichiometric and a post-sintering annealing was conducted in a tube furnace in 4% H₂/Ar gas atmosphere. Prior to reducing, the furnace was purged by 4 h gas flow at a rate of 200 ml/min. The reducing was conducted at 600 °C for 24 h at a gas flow rate of 50 ml/min to render the pellets a stoichiometry of UO_{2.006}. The bulk density of the pellets was measured by an immersing method using DI water as the media. Density was calculated based on weight difference in air and water. The relative density was calculated against a theoretical value of 10.97 g/cc for UO₂ and the porosity of each sample was determined based on relative density.

2.2. Stoichiometry and microstructure of the sintered pellets

X-ray diffractions (XRD) spectra of the sintered pellets were collected by a Panalytical X'Pert XRD system (Westborough, MA, USA) using Cu K_α (λ = 1.5406 Å) as the incident beam at room temperature. The stoichiometry of the sintered pellets was determined from x-ray diffraction collected by The O/U ratio based on the following empirical equation: $a = 5.4705 - 0.132 \cdot x$ [25], where a is the derived lattice parameter and x is the stoichiometry derivation of UO_{2+x} from stoichiometric UO₂.

Microstructure characterization of the sintered UO₂ with controlled microstructure was conducted using a Carl Zeiss Supra 55 (Jana, Germany) field emission SEM. Grain size was determined using a rectangular intercept method following an ASTM E122-88 standard (1992). The average size is given by:

$$D = \left[\frac{4A}{\pi \left(N_i + \frac{N_0}{2} \right)} \right]^{\frac{1}{2}} \quad (1)$$

where A is the area of an arbitrary drawn rectangle, N_i and N_0 are the numbers of grains in the rectangle and on the boundary of the rectangle, respectively. At least two hundred grains were analyzed for each pellet. The grain size uncertainties are standard deviations of the measured grain size for the same pellet from different locations. In the nanoindentation testing, the images and length measurements of the indents were acquired with a FEI Quanta FEG dual beam SEM/FIB system at UC Berkeley in the Biomolecular Nanotechnology Center (BNC). The standard measuring tool was used to perform the measurements of the crack lengths and was calibrated prior to use.

2.3. Nanoindentation testing of the sintered pellets at different temperatures

Nanoindentation testing was performed on the densified UO₂ pellets with controlled microstructure and stoichiometry at 25 °C (298 K), 300 °C (573 K), and 600 °C (873 K) at UC Berkeley with a MicroMaterials platform. The platform was equipped with a nanoindenter that can independently heat the nanoindentation tip and the sample up to 750 °C. This unique ability allows for isothermal contact between the tip and the sample, critical to minimize the thermal drift and enable the measurements of mechanical property, such as hardness and elastic modulus, at elevated temperatures. During the measurement, the instrument is capable of continuously measuring the load *versus* displacement.

For a typical measurement, the indenter was firstly tested on fused silica for calibration. The sample was mounted on a hot stage using Omega 700 cement and the chamber was then purged with UHP Ar overnight with a flow rate of 10 L/min in order to reduce the oxygen particle pressure to the magnitude of 10^{-4} . Then, Ar + 5% H₂ was flowed into the chamber 60–90 mins prior to the testing and maintained thereafter until the end. The tip and the sample were both heated to the desired temperature with a heating rate of 1.6 °C/min. After the desired temperature was reached, the sample was held for 1 additional hour to allow for thermal stabilization. After the thermal stabilization period, the sample would be moved a slight distance (20–30 μm) away, where a test indentation could be performed to evaluate the difference in temperature between the tip surface and the sample surface. This was done by monitoring at the thermal drift of an indent. The temperature of the tip and the sample was deemed satisfactorily the same when the thermal drift of the indent was less than ±0.15 nm/s. The thermal drift was measured by holding at 10% of the max impressing load for 60 s and only the last 60% of the data was used to calculate the drift to remove any artifacts from elastic or plastic behavior at the beginning of the holding period.

During the testing, the nanoindentation was performed in load control mode with a loading time around 20 s, and an unloading time of around 10 s. Approximately the same depth (~800 nm) was maintained for each indentation performed at all temperature levels. The load and the displacement were continuously recorded. To ensure the precision of the indentation, all impressions that had high thermal drifts (>0.2 nm/s) were removed from the dataset. In addition, the dwell time was set as 20 s for the RT indentations, 35 s for 300 °C, and 45 s for 600 °C to ensure that the unloading was completely elastic. At all three temperatures, 5 to 10 indentations were performed on each sample to reduce the experimental error. The reduced modulus was calculated based on formula (2), where E_r is the reduced modulus, β is a geometrical constant on the order of unity, and s is the stiffness of the unloading curve, respectively. The reduced modulus was then converted to elastic modulus using formula (3) proposed by Oliver and Pharr [26]. This formula depicts the relationship between reduced modulus E_r and elastic modulus E , where ν is Poisson's ratio and E_i is elastic modulus of the indenter. The material of the indenter used is cubic boron nitride; therefore, $\nu_i = 0.1$ and $\nu_s = 0.32$ are used for the calculation. The Young's modulus E_i of the indenter is calculated based on the Wachtman's equation [27] shown in formula (4), in which E_0 is a constant representing Young's modulus at absolute zero [28], C is an exponential fitting constant, and T_0 is the characteristic temperature at which Young's modulus shows a linear correlation with temperature. As for the material of the indenter, $E_0 = 681.6$ GPa, $C = 0.0442$, $T_0 = 526.52$ K. This approach takes into account the indenter compliance [29] and can be used to evaluate hardness and Young's modulus without the measurement of contact area [30].

$$E_r = \frac{1}{\beta} \frac{\sqrt{\pi}}{2} \frac{s}{\sqrt{A}} \quad (2)$$

$$\frac{1}{E_r} = \frac{1 - \nu^2}{E} + \frac{1 - \nu_i^2}{E_i} \quad (3)$$

$$E_i = E_0 - C \exp\left(-\frac{T_0}{T}\right) \quad (4)$$

2.4. Microindentation testing

Microindentation testing was performed at 25 °C in order to determine the hardness and to study the crack propagation behavior of samples with various grain sizes and stoichiometries. The micro indenter is a Leco M – 400 Microhardness Tester. The load was kept at 1000 gf (~9.8 N) for 15 s for all indentations. Crack lengths for each indentation were measured based on the SEM images. A schematic of the length measurement is shown in Fig. 1. Similar to nanoindentation, 10 microindentations were performed for each sample. Hardness is calculated using formula (5), where P is the load and a is the arithmetic mean of the diagonal lengths of the indentation. Fracture toughness was calculated based on formula (6) [23,31], where δ is an indenter geometry related parameter, E is elastic modulus, H is hardness, and c is the arithmetic mean of the four crack lengths.

$$H = 1.854 \frac{P}{a^2} \quad (5)$$

$$K_{IC} = \delta \left(\frac{E}{H}\right)^{0.5} \left(\frac{P}{C^{1.5}}\right) \quad (6)$$

3. Results and discussion

3.1. Microstructure control and stoichiometry of the sintered UO₂ by SPS

Fig. 2 shows microstructural analysis of the densified UO₂ pellets as observed by the SEM images acquired from the fractured surface. The chemical stoichiometry of the sintered pellets was determined by X-ray diffraction patterns (data not shown here). Uniform microstructures across the polycrystalline pellets are obtained with different length scales varying from hundreds of nanometers (Fig. 2A) to several microns (Fig. 2B and C), attributing to the fine control of microstructure by SPS process. The

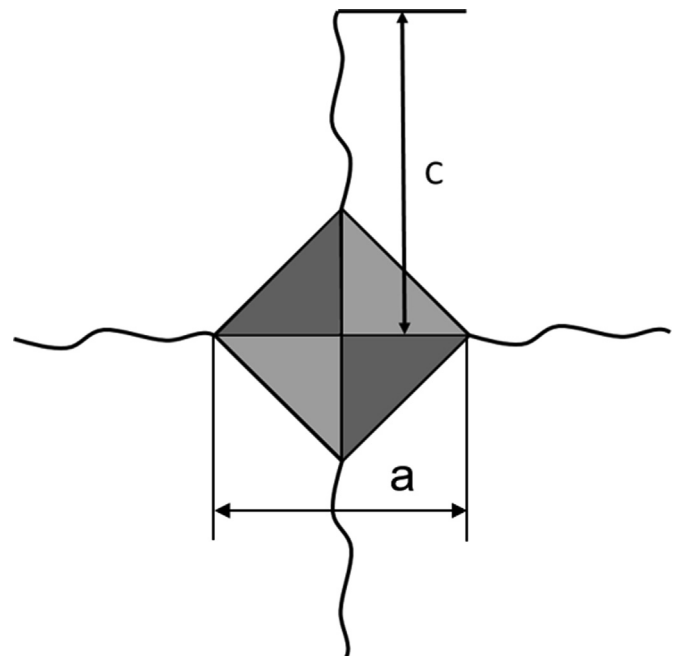


Fig. 1. Schematics of the microindentation.

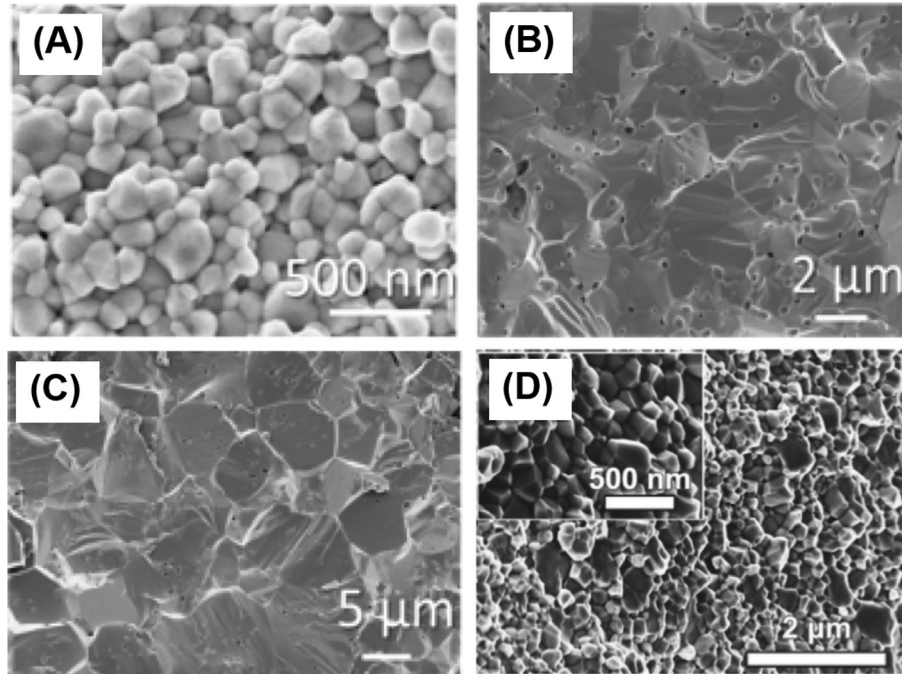


Fig. 2. Synthesized dense UO_2 fuel pellet with various grain sizes: (A) 125 nm stoichiometric UO_2 ; (B) 2 μm stoichiometric UO_2 ; (C) 7 μm stoichiometric UO_2 ; and (D) 165 nm hyperstoichiometry $\text{UO}_{2.11}$.

stoichiometry is controlled to almost identical (close to nearly stoichiometric UO_2) for the densified pellets with different microstructures by the SPS sintering process and also post sintering chemical reduction, and thus the effects of the grain structure on fracture mechanisms and mechanical properties can be determined at similar chemical stoichiometry. Dense nano-sized $\text{UO}_{2.11}$ pellets (Fig. 2D) with hyperstoichiometry (oxygen-enriched) was fabricated with a comparable grain structure (160 nm) as the dense nano- UO_2 pellets (125 nm), and the effects of the oxygen non-stoichiometry on mechanical properties can be explored. The physical properties (grain size and porosity) of different UO_2 pellets for mechanical testing are summarized in Table 1.

The microstructure analysis of the densified UO_2 pellets with different grain structures also reveals distinct variations in fractured surfaces, suggesting different fracture mechanisms. Specifically, for nc- UO_2 , the fractured surface shows typical intergranular fracture with cracking propagation along the grain boundaries as a result of the nano-scale grain structure. The intergranular fracture was also observed in hyper-stoichiometric $\text{UO}_{2.11}$ (Fig. 2D). On the other hand, micron-sized polycrystalline UO_2 pellets show characteristic features of the transgranular fractures, and fractured facets are observed as a result of crack penetration through the grains. The intergranular fracture mechanism suggests better ductility for nano-sized UO_2 as compared with micron-sized counterpart, implying potentially-enhanced fracture toughness for the high burn-up structure formed in oxide fuels upon reactor operation.

Table 1
Summary of sample details for nanoindentation and microindentation testing.

Sample #	Sample type	Porosity	Stoichiometry	Grain Size
1	Nano	3.5%	2.006 ± 0.020	125 ± 7 nm
2	Micron	4.2%	1.996 ± 0.004	1.8 ± 0.2 μm
3	Micron	3.7%	1.979 ± 0.004	7.2 ± 1.2 μm
4	Nano-hyper	1.6%	2.11	165 ± 6 nm

3.2. Hardness and Young's modulus of UO_2 measured by nanoindentation testing

The mechanical properties (hardness and Young's modulus) of the densified UO_2 are determined by nanoindentation as functions of grain structures and temperature. Fig. 3 shows the SEM images for the nanoindentation on the UO_2 pellet (sample #3) with the grain size of 7.2 μm , at different temperatures of 25 °C (a), 300 °C (b), and 600 °C (c), respectively. The hardness and Young's modulus acquired from nanoindentation is summarized below in Tables 2–4.

The temperature dependence of the hardness for sample No. 1 to 3 is shown in Fig. 4A. Two data points (shown as black dots) measured from microindentation testing are also included for comparison. Several observations can be made from this plot. First, hardness decreases exponentially with the increase of temperature, which matches well with the relationship depicted by Kutty [32,33], Sengupta [19], and Basak [34]. The relationship of the hardness and temperature is given as formula (7), where H is hardness, T is temperature in the unit of K , and A and B are intrinsic hardness and thermal softening coefficients, respectively. The negative correlation might be explained by the mechanism of slip at low temperature [35] and increased dislocation activity at high temperature [36].

$$H = A \exp(-BT) \quad (7)$$

Fig. 4B shows the correlation between $\ln H$ and temperature for UO_2 specimens with different grain structures. The linear relationship confirms that hardness is exponentially related with temperature. The values of A and B are extrapolated and listed in Table 5. The intrinsic hardness A is the hardness of material at $T = 0$, and the thermal softening coefficient B describes the hardness decreasing rate when temperature increases. The two mc- UO_2 specimens have very close intrinsic hardness, which is much higher than the reported value [19]. The reason might be due to less porosities for the samples densified by SPS and different measuring

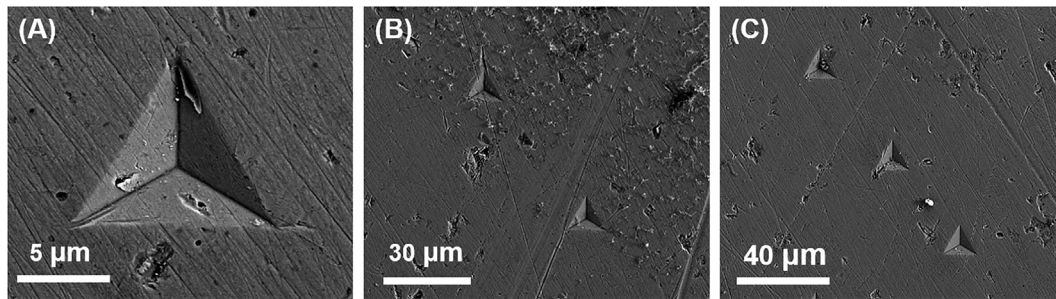


Fig. 3. SEM images showing nanoindentations on the sample No. 3 with 7- μm grain size at (A) 25 °C, (B) 300 °C, (C) 600 °C.

Table 2

Results of the nanoindentation testing on nano-sized UO_2 (sample #1, grain size: 125 nm).

Temperature (K)	Indentation Depth (nm)	Load (mN)	Hardness (GPa)	Reduced Modulus (GPa)	Young's Modulus (GPa)
298	677	100	12.5 ± 0.5	195 ± 3	244 ± 7
573	748	100	7.6 ± 0.3	168 ± 6	200 ± 11
873	864	100	5.9 ± 1.3	149 ± 16	172 ± 26

Table 3

Results of the nanoindentation testing on the micron-sized UO_2 (sample #2, grain size: 2 μm).

Temperature (K)	Indentation Depth (nm)	Load (mN)	Hardness (GPa)	Reduced Modulus (GPa)	Young's Modulus (GPa)
298	1086	200	9.3 ± 0.4	178.3 ± 3.4	216 ± 6
573	790	65	4.3 ± 0.2	165 ± 8	196 ± 14
873	850	35	1.98 ± 0.08	149 ± 16	172 ± 26

Table 4

Results of the nanoindentation testing on the micron-sized UO_2 (sample #3, grain size: 7 μm).

Temperature (K)	Indentation Depth (nm)	Load (mN)	Hardness (GPa)	Reduced Modulus (GPa)	Young's Modulus (GPa)
298	812	100	8.5 ± 0.7	185 ± 12	227 ± 23
573	876	65	4.2 ± 0.4	174 ± 15	210 ± 27
873	888	30	1.8 ± 0.2	154 ± 6	178 ± 11

techniques. It was found that nc- UO_2 has slightly lower intrinsic hardness and small negative thermal softening coefficient than the other two mc-specimens.

Second, the hardness of nc- UO_2 is higher than the other two mc- UO_2 samples, which was also observed by Yang [37], Jung [38], and Nieman [39]. The phenomenon can be well explained by the Hall–Petch effect, which demonstrates that the strength and the hardness of the material can be improved by the grain refinement [40]. Nc- UO_2 introduces more grain boundaries. Various grain orientations at different sides of the grain boundaries will impede the dislocation movement, thus requiring more energy for the deformation and demonstrating higher yield strength of the material. Generally, hardness shows a positive correlation with strength [41], thus refinement of grains will lead to the enhancement of hardness, as long as grain size is larger than the critical grain size.

Fig. 4C shows the variation of hardness with temperature and grain size. It confirms that when grain size increases from nc-scale to mc-scale, hardness decreases drastically due to Hall–Petch effect. Within the mc range, hardness at room temperature has a sharper decreasing rate than at elevated temperature, which matches with Sengupta's findings [19]. The two mc-specimens have very close hardness at elevated temperature, which can be explained by lower boundary strength and easy release of dislocation piled up stress [19].

Lastly, hardness measured in microindentation testing is lower than the value measured by nanoindentation testing, which can be attributed to the variation of load in the nanoindentation and microindentation tests. In the hardness evaluation of UO_2 , $(\text{U}_{0.9}\text{Ce}_{0.1})\text{O}_2$, and $(\text{U}_{0.8}\text{Ce}_{0.2})\text{O}_2$ [20], the authors also noticed that nanohardness is higher than microhardness and they found a negative relationship between hardness and load, i.e., greater hardness with lower load.

Fig. 4D shows the variation of Young's modulus with temperature and grain size. The measured Young's modulus of UO_2 at room temperature is very close to the reported value in Ref. [42]. It can also be noticed that Young's modulus is highly related with temperature and shows a negative correlation [1,27,43]. This might be explained by elastic anisotropy [44] and grain boundary slip [45]. The relationship can be depicted by formula (4), in which T_0 is taken as 135 K as suggested in Ref. [1]. E_0 and A are fitted and shown in Table 6, where E_0 is Young's modulus at absolute zero and A is a fitting constant. The fitted E_0 for two mc-specimens are very close to the reported value and nc-specimen has a slightly higher E_0 than mc-specimens. Young's modulus of the two mc-specimens does not show a strong relationship with grain size, as indicated in the literature [1,42]. As can be noticed from the plot, nc- UO_2 possesses a steeper slope than mc- UO_2 , which indicates that the fitted

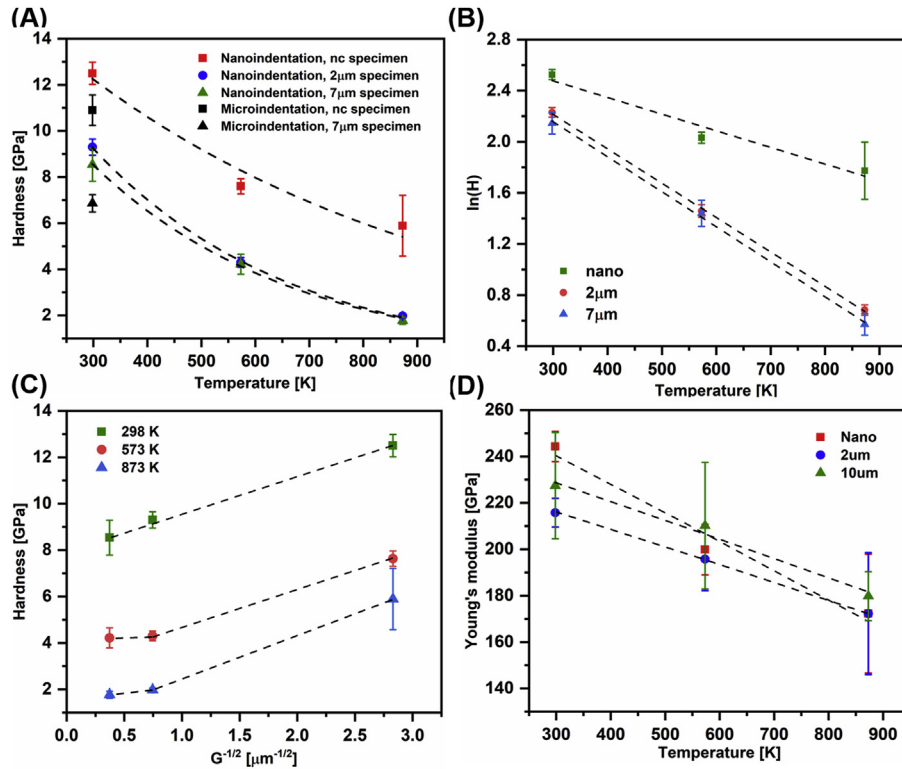


Fig. 4. (A) The temperature dependence of the hardness obtained from nanoindentation testing, along with microindentation testing data for comparison, (B) Linear fitting of $\ln H$ and temperature for UO_2 specimens with various grain sizes, (C) Variation of the hardness with grain size at different temperatures, (D) Variation of Young's modulus of UO_2 with temperature for different grain sizes. Hardness decreases with temperature and nc- UO_2 displays a higher hardness than microcrystalline UO_2 ; while two microcrystalline specimens with different grain sizes have very close hardness. Young's modulus decreases with temperature and there is no a strong relationship between Young's modulus and grain size.

Table 5

Fitted value of intrinsic hardness (A) and thermal softening coefficient (B).

Sample	A (GPa)	B
Nano	17.58	0.001302
2 μm	20.49	0.002689
7 μm	19.65	0.002739

Table 6

Fitted values for A and E_0 for each specimen.

Sample	A	E_0
Nano	0.128	264
2 μm	0.079	231
7 μm	0.085	245

parameter C is larger for nc- UO_2 . Wachtman [27] studied the exponential temperature dependence of oxides and found that the value of B/E_{25} (E_{25} is Young's modulus at 25 °C) is related with the Grüneisen parameter γ , which is a measure of anharmonicity. Polycrystalline sample has a larger value of γ than single crystal sample, which can explain the phenomenon observed here. Nc- UO_2 sample has higher γ than mc- UO_2 sample, thus has a higher decreasing rate than mc- UO_2 when Young's modulus drops with temperature.

3.3. Hardness and fracture toughness of UO_2 measured from micro-indentation testing

Fig. 5 shows the SEM images of the microindentations on three specimens, along with images showing crack propagations. As

suggested in Refs. [46–48], the fracture mode is highly dependent on grain size. Materials with finer grains is very likely to have a fracture mode of intergranular fracture, while transgranular fracture for coarse-grained materials. According to the formula proposed by Petch [49] formula (8), where σ_f is fracture strength, σ_0 is the stress moving dislocations, K is related with fracture initiation energy, and GS is the average grain size, fracture strength has a negative correlation with grain size. Thus the nc-specimen will have more ability to resist fracture. In the current case, the fractography of the mc-specimen displays transgranular fracture with smooth fracture and no sharp edges; while the fractography of the nc-specimen displays intergranular fracture characteristics with jaggy paths.

$$\sigma_f = \sigma_0 + K(GS)^{-\frac{1}{2}} \quad (8)$$

Microhardness and fracture toughness measurements were also performed on sintered UO_2 with different stoichiometry and grain sizes and evaluated with formula (4) and (5). Microhardness for each specimen is summarized in Table 7 and is also plotted in Fig. 6 for better comparison. From the figures, two observations can be made. First, nc-stoichiometric specimen has higher hardness and slightly higher fracture toughness than mc-stoichiometric specimen, matching with the findings of Igata et al. [42], Rice et al. [50], Tapatee et al. [17], and Chunsheng [51]. The higher hardness measured for nc-stoichiometric specimens is consistent with nano-indentation measurement as shown in Fig. 4A. Second, nc-hyperstoichiometric specimen displays higher hardness and fracture toughness than nc-stoichiometric specimen. The enhanced fracture toughness can be explained by the fact that nc-specimen has more grains per volume due to smaller grain size. Thus, more grain

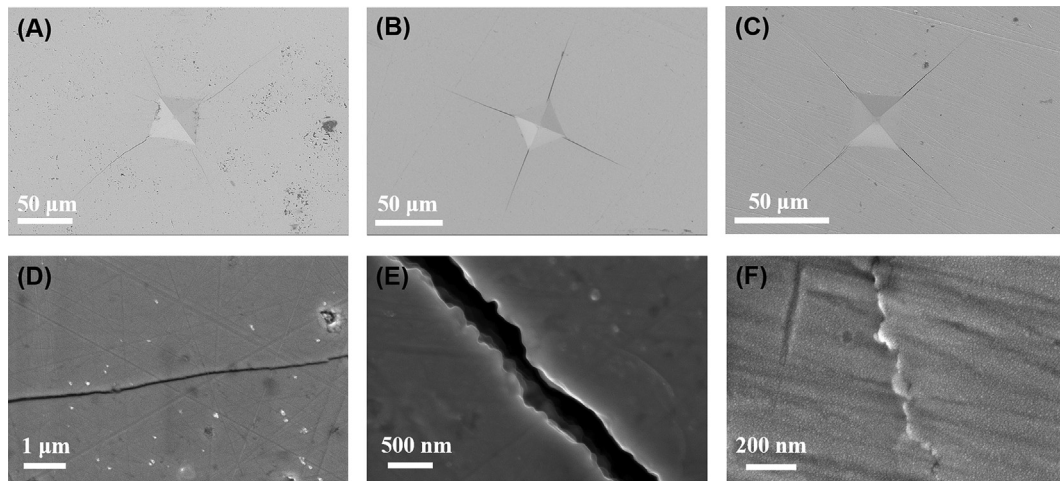


Fig. 5. SEM images for three UO_{2+x} specimens with various stoichiometry and grain sizes. (A) stoichiometric 7- μm UO_2 (sample No. 3), (B) stoichiometric nc- UO_2 (sample No. 1), (C) hyper-stoichiometric nc-specimen (sample No. 4), (D) transgranular fracture in sample No. 3, (E–F) intergranular fracture in sample No. 1 and 4.

Table 7

Hardness and fracture toughness of three specimens with various grain size and stoichiometry.

Sample	Load (gf)	Microhardness (GPa)	Fracture Toughness ($\text{MPa}\cdot\text{m}^{1/2}$)
7 μm	1000	6.8 ± 0.4	1.0 ± 0.1
Nano	1000	10.9 ± 0.7	1.1 ± 0.2
Nano-hyper	1000	12.9 ± 0.1	1.3 ± 0.1

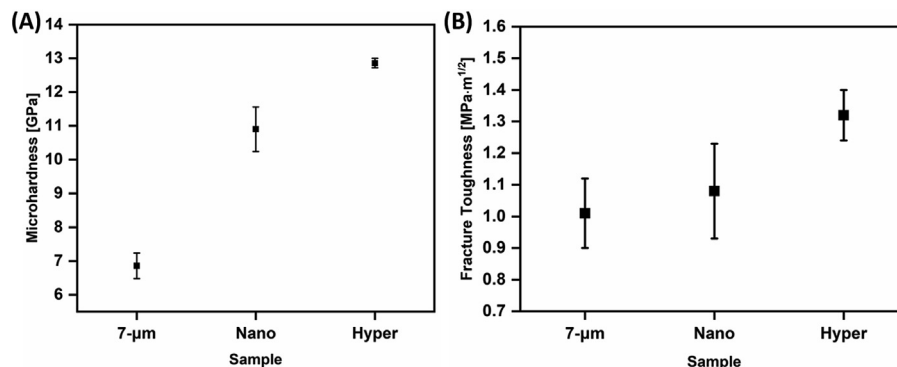


Fig. 6. (A) Microhardness and (B) Fracture toughness of three specimens with various stoichiometry and grain size measured from micro-indentation testing. nc- UO_2 has a higher value than microcrystalline UO_2 , and hyper-stoichiometric UO_2 has a higher value than stoichiometric UO_2 .

boundaries lead to a more complexity of the dislocation structures among grains and will hamper the movement of the dislocations and the propagation of the cracks. When a crack is moving across the grain boundary, it is more difficult for the crack to pass through those grain boundaries with more complex dislocation structures and therefore require more energies. Second, nc-hyper-stoichiometric specimen displays higher hardness and fracture toughness than nc-stoichiometric specimen. It was reported [52] that there is a strong relationship between U/O ratio and hardness. Hardness will rapidly increase when O/U ratio initially increases from 2.00. Surface energy γ can be expressed as a function of fracture toughness K_{IC} as shown in formula (9) [53], where ν is Poisson's ratio and E is Young's modulus. It was also reported in Refs. [53,54] that the excess oxygen will lead to the increase of γ in UO_{2+x} , such that hyper-stoichiometric specimen will possess a higher value of fracture toughness than stoichiometric specimen. More work related to mechanical properties of hyper-

stoichiometric UO_2 at elevated temperatures will be performed in the future and will be compared with stoichiometric UO_2 .

$$2\gamma = \frac{1 - \nu^2}{E} K_{IC}^2 \quad (9)$$

4. Conclusions

In summary, nanoindentation and microindentation testings were conducted on SPS-sintered UO_2 with controlled stoichiometry and grain size. Hardness and Young's modulus at three different temperatures were evaluated during nanoindentation testing, while hardness and fracture toughness at RT were derived from microindentation. Hardness of nc- UO_2 is higher than mc- UO_2 , while mc- UO_2 specimens with different grain sizes have similar hardness. Both hardness and Young's modulus decrease with

temperatures. Results from microindentation testing confirm that nc-UO₂ has a higher hardness and fracture toughness than mc-UO₂ and it can be explained by the theory of grain boundary strengthening. Hyper-stoichiometric UO₂ exhibits higher hardness and fracture toughness than stoichiometric UO₂ and is explained by the impediment of crack propagation induced by excess oxygen atoms and the enhanced fracture surface energy. As the study of mechanical properties on UO₂ with controlled microstructure, stoichiometry, and temperature is limited in the literature, this systematic investigation of hardness, elastic modulus, and fracture toughness using nano- and micro-indentation testing may provide a profound understanding of the relationship among grain size, stoichiometry, temperature and the mechanical properties of UO₂. This work also provides experimental data of mechanical properties and fracture mechanisms to validate the fracture MARMOT model.

Data availability

Data will be made available on request.

Acknowledgements

This work is supported by the U.S. Department of Energy, Office of Nuclear Energy under a Nuclear Engineer University Program (award number: DE-NE0008440). Nano-indentation experiments are supported through a NSUF RTE award (award number: 17-849) under DOE Idaho Operations Office Contract DE-AC07-051D14517 as part of a Nuclear Science User Facilities Experiments.

Appendix A. Supplementary data

Supplementary data to this article can be found online at <https://doi.org/10.1016/j.jnucmat.2019.01.021>.

References

- [1] H. Stehle, H. Assmann, F. Wunderlich, Uranium dioxide properties for LWR fuel rods, *Nucl. Eng. Des.* 33 (2) (1975) 230–260.
- [2] L. Ge, G. Subhash, R.H. Baney, J.S. Tulenko, E. McKenna, Densification of uranium dioxide fuel pellets prepared by spark plasma sintering (SPS), *J. Nucl. Mater.* 435 (1–3) (2013) 1–9.
- [3] V.V. Rondinella, T. Wiss, The high burn-up structure in nuclear fuel, *Mater. Today* 13 (12) (2010) 24–32.
- [4] K. Lassmann, C.T. Walker, J. van de Laar, F. Lindström, Modelling the high burnup UO₂ structure in LWR fuel, *J. Nucl. Mater.* 226 (1–2) (1995) 1–8.
- [5] A.H. Chokshi, A. Rosen, J. Karch, H. Gleiter, On the validity of the hall-petch relationship in nanocrystalline materials, *Scripta Metall.* 23 (10) (1989) 1679–1683.
- [6] C. Suryanarayana, Nanocrystalline materials, *Int. Mater. Rev.* 40 (2) (1995) 41–64.
- [7] N. Wang, Z. Wang, K.T. Aust, U. Erb, Effect of grain size on mechanical properties of nanocrystalline materials, *Acta Metall. Mater.* 43 (2) (1995) 519–528.
- [8] G.A. Malygin, Plasticity and strength of micro- and nanocrystalline materials, *Phys. Solid State* 49 (6) (2007) 1013–1033.
- [9] C. Suryanarayana, C.C. Koch, Nanocrystalline materials – current research and future directions, *Hyperfine Interact.* 130 (1/4) (2000) 5–44.
- [10] Y.Z. Wang, G.W. Qiao, X.D. Liu, B.Z. Ding, Z.Q. Hu, Electrical resistivity of nanocrystalline Fe-Cu-Si-B alloys obtained by crystallization of the amorphous alloy, *Mater. Lett.* 17 (3–4) (1993) 152–154.
- [11] E.O. Hall, The deformation and ageing of mild steel: III discussion of results, *Proc. Phys. Soc. B* 64 (9) (1951) 747–753.
- [12] C. Suryanarayana, D. Mukhopadhyay, S.N. Patankar, F.H. Froes, Grain size effects in nanocrystalline materials, *J. Mater. Res.* 7 (08) (2011) 2114–2118.
- [13] I. Amato, R.L. Colombo, A.M.P. Balzari, Hot-pressing of uranium dioxide, *J. Nucl. Mater.* 20 (2) (1966) 210–214.
- [14] J.H. Yang, K.W. Song, Y.W. Lee, J.H. Kim, K.W. Kang, K.S. Kim, Y.H. Jung, Microwave process for sintering of uranium dioxide, *J. Nucl. Mater.* 325 (2–3) (2004) 210–216.
- [15] T. Yao, S.M. Scott, G. Xin, B. Gong, J. Lian, Dense nanocrystalline UO_{2+x} fuel pellets synthesized by high pressure spark plasma sintering, *J. Am. Ceram. Soc.* 101 (3) (2017) 1105–1115.
- [16] B. Gong, T. Yao, C. Lu, P. Xu, E. Lahoda, J. Lian, Consolidation of commercial-size UO₂ fuel pellets using spark plasma sintering and microstructure/microchemical analysis, *MRS Communications* (2018) 1–9.
- [17] T.K. Roy, Assessing hardness and fracture toughness in sintered zinc oxide ceramics through indentation technique, *Mater. Sci. Eng.* 640 (2015) 267–274.
- [18] J. Spino, J. Cobos-Sabate, F. Rousseau, Room-temperature microindentation behaviour of LWR-fuels, part 1: fuel microhardness, *J. Nucl. Mater.* 322 (2–3) (2003) 204–216.
- [19] A.K. Sengupta, C.B. Basak, T. Jarvis, R.K. Bhagat, V.D. Pandey, S. Majumdar, Effect of titania addition on hot hardness of UO₂, *J. Nucl. Mater.* 325 (2–3) (2004) 141–147.
- [20] K. Kurosaki, Y. Saito, H. Muta, M. Uno, S. Yamanaka, Nanoindentation studies of UO₂ and (U,Ce)O₂, *J. Alloy. Comp.* 381 (1–2) (2004) 240–244.
- [21] Y. Gu, T. Nakamura, L. Prchlik, S. Sampath, J. Wallace, Micro-indentation and inverse analysis to characterize elastic–plastic graded materials, *Mater. Sci. Eng.* 345 (1–2) (2003) 223–233.
- [22] J. Menčík, D. Munz, E. Quandt, E.R. Weppelmann, M.V. Swain, Determination of elastic modulus of thin layers using nanoindentation, *J. Mater. Res.* 12 (09) (2011) 2475–2484.
- [23] K. Kapoor, A. Ahmad, A. Lakshminarayana, G.V.S. Hemanth Rao, Fracture properties of sintered UO₂ ceramic pellets with duplex microstructure, *J. Nucl. Mater.* 366 (1–2) (2007) 87–98.
- [24] T. Yao, K. Mo, D. Yun, S. Nanda, A.M. Yacout, J. Lian, Grain growth and pore coarsening in dense nano-crystalline UO_{2+x} fuel pellets, *J. Am. Ceram. Soc.* 100 (6) (2017) 2651–2658.
- [25] K. Teske, H. Ullmann, D. Rettig, Investigation of the oxygen activity of oxide fuels and fuel-fission product systems by solid electrolyte techniques. Part I: qualification and limitations of the method, *J. Nucl. Mater.* 116 (2–3) (1983) 260–266.
- [26] W.C. Oliver, G.M. Pharr, An improved technique for determining hardness and elastic modulus using load and displacement sensing indentation experiments, *J. Mater. Res.* 7 (06) (2011) 1564–1583.
- [27] J.B. Wachtman, W.E. Tefft, D.G. Lam, C.S. Apstein, Exponential temperature dependence of young's modulus for several oxides, *Phys. Rev.* 122 (6) (1961) 1754–1759.
- [28] R.A. Wolfe, S.F. Kaufman, MECHANICAL PROPERTIES OF OXIDE FUELS, 1967.
- [29] I.S. Choi, O. Kraft, R. Schwaiger, Validity of the reduced modulus concept to describe indentation loading response for elastoplastic materials with sharp indenters, *J. Mater. Res.* 24 (03) (2011) 998–1006.
- [30] A. Bolshakov, G.M. Pharr, Influences of pileup on the measurement of mechanical properties by load and depth sensing indentation techniques, *J. Mater. Res.* 13 (04) (2011) 1049–1058.
- [31] G.R. Anstis, P. Chantikul, B.R. Lawn, D.B. Marshall, A critical evaluation of indentation techniques for measuring fracture toughness: I, direct crack measurements, *J. Am. Ceram. Soc.* 64 (9) (1981) 533–538.
- [32] T.R.G. Kutty, T. Jarvis, C. Ganguly, Hot hardness and indentation creep studies on Zr-1Nb-1Sn-0.1Fe alloy, *J. Nucl. Mater.* 246 (2–3) (1997) 189–195.
- [33] T.R.G. Kutty, K. Ravi, C. Ganguly, Studies on hot hardness of Zr and its alloys for nuclear reactors, *J. Nucl. Mater.* 265 (1–2) (1999) 91–99.
- [34] U. Basak, A.K. Sengupta, C. Ganguly, Hot hardness and thermal conductivity of ThO₂-PuO₂ and ThO₂-UO₂ sintered pellets, *J. Mater. Sci. Lett.* 8 (4) (1989) 449–450.
- [35] G. Sharma, R.V. Ramanujan, T.R.G. Kutty, G.P. Tiwari, Hot hardness and indentation creep studies of a Fe–28Al–3Cr–0.2C alloy, *Mater. Sci. Eng.* 278 (1–2) (2000) 106–112.
- [36] Y.D. Han, H.Y. Jing, S.M.L. Nai, L.Y. Xu, C.M. Tan, J. Wei, Temperature dependence of creep and hardness of Sn-Ag-Cu lead-free solder, *J. Electron. Mater.* 39 (2) (2009) 223–229.
- [37] B. Yang, H. Vehoff, Dependence of nanohardness upon indentation size and grain size – a local examination of the interaction between dislocations and grain boundaries, *Acta Mater.* 55 (3) (2007) 849–856.
- [38] B.B. Jung, H.K. Lee, H.C. Park, Effect of grain size on the indentation hardness for polycrystalline materials by the modified strain gradient theory, *Int. J. Solid Struct.* 50 (18) (2013) 2719–2724.
- [39] G.W. Nieman, J.R. Weertman, R.W. Siegel, Mechanical behavior of nanocrystalline Cu and Pd, *J. Mater. Res.* 6 (05) (2011) 1012–1027.
- [40] N. Hansen, Hall–Petch relation and boundary strengthening, *Scripta Mater.* 51 (8) (2004) 801–806.
- [41] P. Zhang, S.X. Li, Z.F. Zhang, General relationship between strength and hardness, *Mater. Sci. Eng.* 529 (2011) 62–73.
- [42] N. Igata, K. Domoto, Fracture stress and elastic modulus of uranium dioxide including excess oxygen, *J. Nucl. Mater.* 45 (4) (1973) 317–322.
- [43] O.L. Anderson, Derivation of wachtmann's equation for the temperature dependence of elastic moduli of oxide compounds, *Phys. Rev.* 144 (2) (1966) 553–557.
- [44] R.W. Rice, Possible effects of elastic anisotropy on mechanical properties of ceramics, *J. Mater. Sci. Lett.* 13 (17) (1994) 1261–1266.
- [45] J.B. Wachtman, D.G. Lam, Young's modulus of various refractory materials as a function of temperature, *J. Am. Ceram. Soc.* 42 (5) (1959) 254–260.
- [46] B. Mussler, M.V. Swain, N. Claussen, Dependence of fracture toughness of alumina on grain size and test technique, *J. Am. Ceram. Soc.* 65 (11) (1982) 566–572.
- [47] J.R.G. Evans, R. Stevens, S.R. Tan, The thermal shock of β-alumina, *J. Mater. Sci.* 19 (11) (1984) 3692–3701.
- [48] M. Oguma, Microstructure effects on fracture strength of UO₂ fuel pellets,

- J. Nucl. Sci. Technol. 19 (12) (1982) 1005–1014.
- [49] N.J. Petch, The cleavage strength of polycrystals, The Journal of the Iron and Steel Institute 173 (5) (1953) 25–28.
- [50] R.W. Rice, C.C. Wu, F. Boichelt, Hardness-grain-size relations in ceramics, J. Am. Ceram. Soc. 77 (10) (1994) 2539–2553.
- [51] C. Lu, R. Danzer, F.D. Fischer, Scaling of fracture strength in ZnO: effects of pore/grain-size interaction and porosity, J. Eur. Ceram. Soc. 24 (14) (2004) 3643–3651.
- [52] B.E. Schaner, Metallographic determination of the UO₂-U₄O₉ phase diagram, J. Nucl. Mater. 2 (2) (1960) 110–120.
- [53] T. Inoue, H. Matzke, Fracture surface energy of UO₂ and ThO₂ containing additives, J. Nucl. Sci. Technol. 17 (12) (1980) 908–912.
- [54] H. Matzke, T. Inoue, R. Warren, The surface energy of UO₂ as determined by hertzian indentation, J. Nucl. Mater. 91 (1) (1980) 205–220.
- [55] V.V. Rondinella, T. Wiss, The high burn-up structure in nuclear fuel, Mater. Today 13 (12) (2010) 24–32.
- [56] Y.B. Miao, T.K. Yao, J. Lian, S.F. Zhu, S. Bhattacharya, A. Oaks, A.M. Yacout, K. Mo, Nano-crystallization induced by high-energy heavy ion irradiation in UO₂, Scripta Mater. 155 (2018) 169–174.
- [57] C.E. Carlton, P.J. Ferreira, What is behind the inverse Hall-Petch effect in nanocrystalline materials? Acta Mater. 55 (11) (2007) 3749–3756.
- [58] W. He, S.D. Bhole, D. Chen, Modeling the dependence of strength on grain sizes in nanocrystalline materials, Sci. Technol. Adv. Mater. 9 (1) (2008) 015003.
- [59] H. Ryou, J.W. Drazin, K.J. Wahl, S.B. Qadri, E.P. Gorzkowski, B.N. Feigelson, J.A. Wollmershauser, Below the Hall-Petch Limit in Nanocrystalline Ceramics, ACS Nano 12 (4) (2018) 3083–3094.